https://doi.org/10.5194/essd-2022-467
Preprint. Discussion started: 11 January 2023

Open Access Earth System Science Data Discussions

Measurements and modeling of water levels, currents, density and wave climate on a semi-enclosed tidal bay: Cádiz (SW Spain)

Carmen Zarzuelo[1], Alejandro López-Ruiz[1], María Bermúdez[2], and Miguel Ortega-Sánchez[2]

[1]Departamento de Ingeniería Aeroespacial y Mecánica de Fluidos, Universidad de Sevilla, Camino de los Descubrimientos s/n, 41092, Seville, Spain
[2]Andalusian Institute for Earth System Research, University of Granada, Avda. del Mediterráneo, s/n, 18006 Granada, Spain

Correspondence: Carmen Zarzuelo (czarzuelo@us.es)

Abstract. Estuarine dynamics are highly complex as a result of the temperature and salinity gradients, as well as the multiple interactions between atmospheric, maritime and hydrological forcing agents. Given the environmental and socioeconomic importance of estuaries and their current and future threats due to human interventions and climate change, it is of vital importance to characterize these dynamics, monitor their evolution and quantify the expected impacts derived from climate change. This paper presents a hybrid database combining data obtained in six field surveys (in 2012, 2013 and 2015) and results from a physically-based 3D numerical model for the Bay of Cádiz (southern Spain), a highly anthropized mesotidal estuary. The 3D dataset includes water levels, currents, density and wave climate, allowing for an analysis of bay dynamics at different time scales ranging from intratidal processes to seasonal variabilities. The results offer an example of the potential uses of the dataset and include (1) an assessment of the spatial and seasonal variability of the estuarine dynamics and (2) an analysis of the effects of severe weather events. These examples provide convincing evidence regarding how the dataset can be employed in multiple research fields and applications, including ocean-bay interactions, water exchange between basins, long- and short-wave propagation along creek systems and energy extraction of tidal waves. Therefore, this hybrid dataset may be of significant interest for stakeholders and scientists from different sectors (water engineering, ecology, urban development, energy, etc.) working on the environmental management of the Gulf of Cádiz and other tidally-dominated shallow bays. It can also serve as a benchmark test for numerical hydrodynamic models, infrastructure intervention assessments (e.g., dikes or breakwaters) or renewable energy conversion system models.

1 Introduction

An estuary is a partially enclosed coastal water body where freshwater from rivers and streams mixes with saltwater from the ocean (Alahmed et al., 2022). Although influenced by tides, estuaries are frequently protected from the full force of ocean waves, winds and storms (Eryani and Nurhamidah, 2020). The sheltered waters of estuaries also support freshwater and saltwater marshes, swamps, sandy beaches, mud and sand flats, rocky shores, oyster reefs, mangrove forests, river deltas, tidal pools and seagrass beds, which increase the diversity of the environment (Hopkinson et al., 2019; Hobohm et al., 2021). Moreover, wetland plants and soils also act as natural buffers between the land and ocean, absorbing flooded waters and dissipating storm surges (Asari et al., 2021). The protected coastal waters of estuaries also support important public infrastructure, serving

https://doi.org/10.5194/essd-2022-467
Preprint. Discussion started: 11 January 2023

as harbors and ports vital for shipping and transportation, which must be carefully managed to ensure the sustainability and protection of this natural resource (Allison et al., 2020).

The complexity and the environmental and socioeconomic importance of the estuaries described above highlight the need for a detailed characterization of the dynamics of these coastal systems. This information will be even more important in upcoming years and decades, considering the expected impacts of sea level rise due to global warming and climate change in these areas (Haasnoot et al., 2019). Currently, there are three main approaches for characterizing estuaries: (1) physical models, (2) field data, and (3) physically-based numerical modeling. Physical models replicate coastal systems at a reduced scale so that the major dominant forces acting are reproduced (Reeve et al., 2018). Although these models are extensively applied in the design of major hydraulic engineering works and greatly enhance our understanding of fluvial, estuarine and coastal processes (Weisscher et al., 2020), the characteristics of estuarine dynamics complicate their use; complex geometries, a significant number of different forcings acting simultaneously, and water density gradients have to be considered. Furthermore, the conditions required to appropriately model the substrate, sediment and biota are difficult to reproduce in the laboratory.

Field data are obtained through multiparameter and multiscale environmental monitoring at a limited number of discrete locations where appropriate scientific instrumentation can be deployed (Garel and Ferreira, 2015). With this approach, hydrodynamic variables and water properties such as water levels, currents, salinity and/or water density can be measured. The usefulness of these data in characterizing estuarine dynamics relies primarily on the design of the deployment (type, number, location and setup of the equipment), the length of the survey, and the representativeness of the meteorological, atmospheric, maritime and hydrological conditions during the selected period of time. Despite providing the most realistic characterization of the estuarine dynamics currently available, field data have severe limitations due to the isolated locations of the environmental monitoring devices and the limited variables and conditions that can be measured.

Physically-based numerical models overcome these limitations by resolving the conservation equations that are approximations of laws for water flow and/or sediment transport (e.g., Meyer-Peter and Müller (1948); Van Rijn (2007); Baar et al. (2019)). These equations are solved in a spatial domain that can cover complete estuarine areas with spatial resolutions up to tens of meters. The interest in such models lies not only in the transition from isolated to spatially distributed data but also in the analysis of conditions that did not occur during the observation period, including prospective conditions resulting from a changing climate (e.g., Yang et al. (2015); Del-Rosal-Salido et al. (2021)), as these models enable full control of the initial and boundary conditions (Weisscher et al., 2020) in contrast to field data. The main limitation of numerical modeling comes from the significant number of model parameters (e.g., bed friction, viscosity, diffusivity) that have to be adjusted to adequately reproduce the hydrodynamic and transport processes. This problem is solved by calibrating and testing these parameters using field data and exploring the sensitivity to changes in their values (van Maren and Cronin, 2016). Hence, field data and numerical modeling are complementary approaches that can be used simultaneously to analyze estuarine dynamics, to adequately reproduce the processes observed in nature, and in turn to allow prognostic and extreme event analysis.

This paper presents a hybrid dataset developed to characterize the hydrodynamics, salinity and temperature distributions in the mesotidal estuary of the Bay of Cádiz (southern Spain). This bay is a paradigmatic example of a complex geometry, tidally-dominated bay where different basins are connected through narrow channels and waves and river discharges have limited

https://doi.org/10.5194/essd-2022-467
Preprint. Discussion started: 11 January 2023

influence. Similar estuaries can be found worldwide, such as San Francisco Bay (Gartner and Walters, 1986), Jiaozhou Bay (Li et al., 2014), the St Lucia estuarine lake (Schoen et al., 2014), and the Sylt-Romo Bight (Purkiani et al., 2016). The dataset includes both field data and numerical modeling results that were obtained for the study area during the last decade. In addition to analyzing the general hydrodynamics and transport processes in the bay (Zarzuelo et al., 2021), the dataset was used to study the impact of human interventions on estuarine dynamics (Zarzuelo et al., 2015) and the tidal energy potential in the area (Zarzuelo et al., 2018). With the description presented here and its open-source publication, the dataset aims to provide treated and formatted hydrodynamic data for engineers and researchers working on the environmental management of the Gulf and Bay of Cádiz, including aspects such as water quality (Jiménez-Arias et al., 2020; Besada et al., 2022), ecosystem functioning (Miró et al., 2020; Haro et al., 2022) or energy assessments (Zarzuelo et al., 2018; Legaz et al., 2020). These data may also be of interest to modelers; in particular, they can be used as a benchmark test case for numerical hydrodynamic models, as a reference for human intervention alternatives (e.g., piles, dikes or breakwaters), or as a basis for modeling renewable energy conversion systems. In addition, the dataset may be of interest for scientists aiming to compare the behavior of different estuarine areas.

2 Area description

The Bay of Cádiz is a mesotidal, mixed energy and well-stratified estuary (Zarzuelo et al., 2015, 2017, 2020) in southern Spain, characterized by a temperate climate. The bay consists of three areas (A, B and C in Fig.1) and a zone of tidal flats and marshes, with a total extension of 140 km2. The outer basin (A), with an area of 70 km^2, is characterized by mild slopes and depths ranging between 5-10 m. This area is the most exposed to wave action due to its opening to the Atlantic Ocean and is also connected with the estuaries of the San Pedro and Guadalete rivers. The inner basin (C) has an extension of 50 km2, with intertidal areas that give rise to an area of gentle slopes, which is reconnected to the Atlantic Ocean through the 17 km-long tidal creeks of Carracas and Sancti-Petri (Zarzuelo et al., 2018, 2020). Finally, the Puntales channel (B) connects the outer and inner basins with dimensions of 3.1 km and 1.7 km in length and width, respectively. This latter area exhibits the greatest depths (up to 18 m) and corresponds to the zone where most recent human interventions are sheltered. The bay has tidal ranges of approximately 2-4 m (neap and spring tides, respectively) and a moderate wave climate that propagates mainly from the Atlantic Ocean with a limited incursion inside the bay. The influence of freshwater discharges is weak since the mean discharge rates are approximately 20 m^3/s compared to a tidal prism of 10^5 m^3/s. With these characteristics, the Bay of Cádiz is considered an example of tidally-dominated, shallow, semi-enclosed bays (Kitheka, 1997; LEE et al., 1997; Newton et al., 2014; Shang et al., 2019).

The estuary contains extensive areas of intertidal sand and mudflats that support a variety of characteristic benthic fauna depending on the nature of the substrate. In its inner basin and around the creeks of Carracas and Sancti-Petri, there are also extensive areas of mudflats. This space, dominated by swamps, marshes, and salt flats, is characterized by an astounding wealth of biodiversity, with a long historical tradition of salt mining. This area has undergone a major transformation due to progressive sedimentary infill conditioned by the important biosedimentary role of vegetation, which often controls the morphological evolution of these tidal environments (D'Alpaos, 2011). At the same time, a significant part of the emerged

https://doi.org/10.5194/essd-2022-467
Preprint. Discussion started: 11 January 2023

marshes within the Bay of Cádiz has been almost completely anthropized over the past 60 years (Gracia et al., 2017). In recent years, many of the structures of old salt marshes have disappeared as a result of the intense transformation that is being carried out in the area.

Since the twentieth century, human interventions such as ports, bridges or salt marshes have been developed to improve the economic and social activities within the bay and its surroundings. The vast majority of these interventions are located in the Puntales channel (Zarzuelo et al., 2015), interfering with the exchange of water, heat and sediment between the outer and inner basins (Zarzuelo et al., 2021).

3 Methods

To analyze the dynamics of the Bay of Cádiz, two methods were used: (1) a combination of 3 bottom-mounted and 3 vessel-towed field surveys that provided real data with high temporal resolution and (2) a 13-month 3D numerical simulation that was calibrated and tested with the field data. This latter simulation provides high spatial resolution data for a longer time period for which variabilities down to seasonal scales can be analyzed. The combination of both methods allows us to analyze the hydrodynamic and morphodynamic behavior of the Bay of Cádiz on a global scale, which was the main milestone of the Project P09-TEP-4630 (funded by the Andalusian Regional Government) that financially supported the study to obtain this hybrid database.

3.1 Design of the field surveys

More than 20 instruments during 6 different surveys were used to measure water levels, currents, water density and conductivity, and wave conditions. The total length of the records considering all the surveys exceeds 8 months. The two types of field surveys designed, bottom-mounted and vessel-towed, are described within the next sections.

3.1.1 Bottom-mounted observations

Three field surveys using bottom-mounted instruments were carried out. These surveys were designed to have short- to mid-term time periods with real data that could (1) characterize the dynamics of the bay and (2) calibrate the numerical model considering a wide range of different tidal, wave, wind and weather conditions. The three deployments were as follows:

- Mounted *Field2012* (22-12-2011 to 22-05-2012): Twelve instruments were anchored in 8 positions distributed along the bay and inside the creeks (see Table 1 and Fig.1b). Concrete blocks were used to secure the instruments on the seabed and avoid displacements. This initial survey was planned to characterize the dynamics of the three main areas of the bay (A, B and C in Fig.1b) and the tidal creeks. Furthermore, data were also used to assess the balance and water exchange between the basins and the creeks and to characterize the effects of extreme wind and wave events that frequently occur during the winter season on the dynamics of the bay.

https://doi.org/10.5194/essd-2022-467
Preprint. Discussion started: 11 January 2023

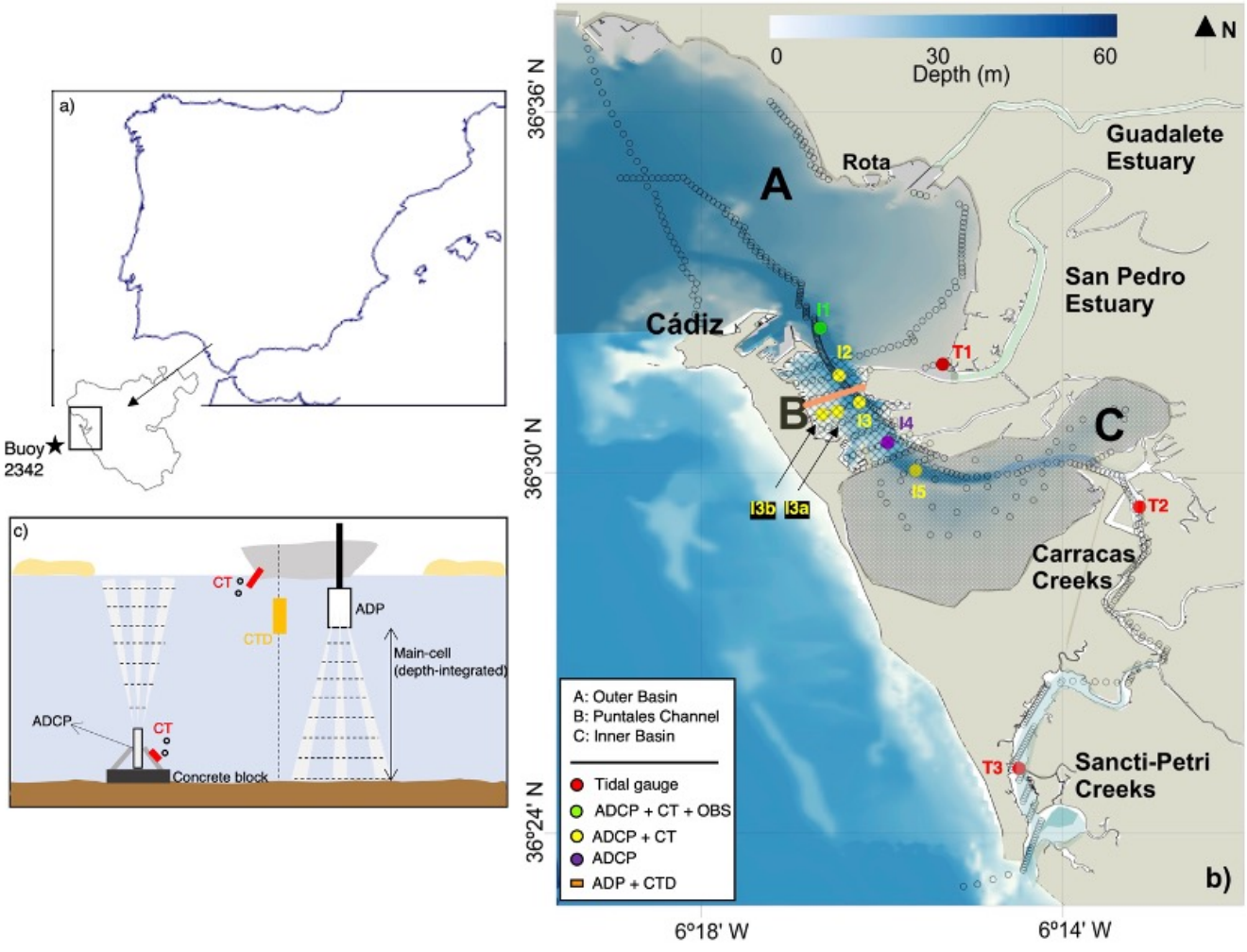

Figure 1. Location (a-b) and description (c) of the monitoring system. The Bay of Cádiz (a) is located on the southern Iberian Peninsula. The locations (b) of the measuring stations are indicated in colored circles, and the cross-sectional surveys are indicated in orange rectangles. The locations of the model data are represented in empty circles. The equipment of the station (c) includes a multiparametric probe (CT and CTD) and an acoustic Doppler current profiler (ADP).Details on the sources of the elevation data depicted in (b) are given in section 3.2.1.

– Mounted *Field2013* (25-05-2013 to 28-08-2013): In this second survey, 6 instruments were anchored in 3 locations distributed along a cross-section of the Puntales channel to characterize the water exchange between the outer basin and the channel itself (see Table 1 and zone B in Fig.1b). In this case, metal tripods were used to secure the instruments on the seabed. After Field2012, it was observed that the main exchange section was the connection between the outer basin and the Puntales channel. Therefore, this survey was designed with 3 locations evenly distributed along a section just at the entrance of the channel.

https://doi.org/10.5194/essd-2022-467
Preprint. Discussion started: 11 January 2023

– Mounted *Field2015* (16-09-2015-23-09-2015): Finally, as results provided by the numerical model suggested that the bay behaves as an inverse estuary, 4 instruments were anchored using tripods in 2 locations to observe heat exchange differences and characterize the water exchange between the Puntales channel and inner basin (Table 1 and Fig.1b).

As shown in Table 1, three different instruments were used during these surveys. Acoustic Doppler current profilers (ADCPs) measured surface pressure, bottom temperature and velocities along the entire water column. From these measured variables, the energy spectrum was assessed to obtain the wave height, peak period and wave direction. All acoustic signals were emitted at 1 Hz from three beams inclined 25° from the vertical and equally spaced 120°. The ADCPs included a high-resolution pressure sensor, as well as compass/tilt and temperature sensors. The distance from the base of the concrete block (tripod) to the top of the ADCPs was 0.3 m (0.8 m). The three flow velocity components (east, north, and vertical) were measured in cells of different thicknesses (multicell data, hereafter) along the water column (Table 1). In addition, the depth-integrated velocities were measured in a cell (main cell data, hereafter) whose vertical extent was automatically adjusted near the surface based on pressure records. Both the main and multicell measurements started at a blanking distance above the instrument and thus at different distances above the bottom (see Table 1). In addition, this distance varied with time due to changes in bed elevation, particularly those resulting from the burial and tilting of the mooring structure (Lobo et al., 2004; Morales et al., 2006; Garel and Ferreira, 2015).

The conductivity-temperature sensors (CTs) measured bottom temperature and conductivity (see Table 1), which could later be converted to salinity values. They recorded data every 15 minutes to be in line with the ADCP data. The optical backscatter sensor (OBS) measured turbidity at the bottom; it shared its configuration with the ADCP since they were nested. Finally, the tide gauges only measured pressure, with 10 sec bursts every 15 min (1 Hz). For more details on the configurations of each field survey, see Table 1.

3.1.2 Vessel-towed observations

As a result of the first bottom-mounted survey (Field2012), important exchange flows were identified between the Inner and Outer basins through the Puntales channel. To analyze these flows in detail, three vessel-towed continuous surveys were conducted in 2013 (2) and 2015 (1) during a tidal cycle at a cross-section of this channel:

– 2013: Two 13 h long acoustic Doppler profiler (ADP) surveys were performed during neap (7 July, Neap2013) and spring (22 August, Spring2013) tides across the Puntales channel (orange line-Fig.1b) to capture the seasonal variability and the water exchange between the outer basin and the channel. In addition, a conductivity-temperature-depth instrument (CTD SeaBird SBE19+, 4 samples at 1 Hz), plus a Wetlabs fluorometer and OBS turbidometer, mounted on a towed Guildline MiniBat undulator, enabled rapid sampling at five extra locations across the transect. Towing at approximately 5 knots provided vertical profiles roughly spaced 200 m every 2.2 hours. Samples of water were also taken to calibrate the sediment suspension in every CTD profile.

https://doi.org/10.5194/essd-2022-467
Preprint. Discussion started: 11 January 2023

– 2015: One 13 h long survey was performed during neap (22 September, Neap2015) tides across the same transect (orange line-Fig.1b) defined in 2013 to capture possible changes produced by the new bridge (seaward of orange line-Fig.1b) built in the Puntales channel between 2007 and 2015 and to assess the temporal variations between 2013 and 2015.

Underway velocity profiles were recorded with a boat-mounted 1200 kHz ADP in 50 cm bins at 120 pings per ensemble during one complete tidal cycle. Navigation was carried out with a global positioning system (GPS). In 2013, a total of 23 transects for neap tides and 24 for spring tides were sampled, while in 2015, a total of 25 transects were sampled for neap tides. The transect data were organized in vertically- and horizontally-uniform grids across the channel.

3.1.3 Post-processing data

After exporting the data from the instruments, errors were eliminated by post-processing. First, a screening compared data in accordance with the battery life. Then, the compass (<0.1°) was corrected by comparison with heading, tilting and rolling (<1°), which causes deviations in the directions of the variables. In addition, the instrumentation was checked for any turning that could have distorted the information. Finally, a comparison between the pressure data and the water column was made to remove the cells that remained above the free surface (or to eliminate the influence of atmospheric pressure).

After sieving the data, pressure was converted to free surface elevation following Nielsen (1989). Moreover, the spectra and the directional spectrum were calculated to obtain the significant wave height, peak period and wave direction (O'brien, 1993). In this procedure, the nonlinear wave portion is low-pass filtered from the original bottom pressure data prior to estimating surface wave values. The filter cutoff is determined for each wave burst after fitting a Pearson spectrum.

Temperature and salinity CTD data were post-processed by applying standard Seabird software and MATLAB routines. At this stage, peaks were removed, 1 dbar averages were calculated, and the downcast profiles of temperature and salinity were corrected with regression analysis. Once the salinity is known, the density is calculated. Suspended sediment concentration (SSC) was derived from OBS (e.g., Downing (2006)) measurements via calibration with suspended matter concentrations gravimetrically determined from water samples. The OBS calibration was accomplished by cross-correlation between the instrument readings and the SSCs obtained from water samples.

The shipboard ADP data were processed to correct the heading errors and then averaged over intervals of 1 min and 1 m depth to provide higher spatial resolution. The ADP time series were edited for outliers, and small gaps were filled by interpolation with a cubic spline. The data sampled more often than once per hour were averaged to 1-h intervals. Currents were rotated into east–west and north–south basin components. The axis directions were determined by examination of the principal axes of the space variability and the orientation of the local bathymetry.

3.2 Numerical modelling

The 3D numerical modeling was performed using DELFT3D, a model developed for the coupled simulation of long and shortwave dynamics, sediment transport and heat fluxes, among other processes. Its subgrid approach for high-resolution bathymetry representation on unstructured grids (Lesser et al., 2004) makes it suitable to simulate hydrodynamics in complex

https://doi.org/10.5194/essd-2022-467
Preprint. Discussion started: 11 January 2023

estuaries such as the Bay of Cádiz. The model, fed with tidal harmonics, wind forcings, wave climate and heat fluxes, provides water levels, currents, density and wave climate with high spatial (both horizontal and vertical) and temporal resolutions. For the conceptual description of the model, the reader is referred to Zarzuelo et al. (2021).

3.2.1 Model set-up

The hydrodynamic and shortwave propagation Delft3D modules were employed. The hydrodynamic module was used to solve the two-dimensional depth-averaged shallow water equations (SWE), the advection-diffusion equation for salt and heat transport, and an equation of state to assess the water density. For this module, water level boundary conditions were defined as astronomical forcings using the 18 main tidal harmonics in the area (M2, S2, SA, Q1, O1, P1, K1, 2N2, MU2, N2, NU2, L2, T2, R2, K2, MN4, M4, and MS4) obtained from the Oregon State Tidal Prediction model (Egbert y Erofeeca, 2002). For the transport boundary conditions, 3 h-interval data of salinity and temperature from Buoy 2342 (Puertos del Estado, Spanish Ministry of Public Works; Fig.1c) were used. Despite their scarce influence, average discharges from the two main rivers (Guadalete and San Pedro) were included as source terms considering their temperature and salinity (data provided by the Andalusian Regional Government). The ocean heat flux model of Delft3D (Gill and Adrian, 1982; Lane, 1989) was used to account for the atmosphere-ocean heat exchange with spatially uniform daily averaged data of solar radiation, air temperature and humidity, and cloudiness (also obtained from the Andalusian Regional Government). Finally, spatially uniform 1 h-interval wind data from Buoy 2342 were used to estimate the wind contribution to the momentum equation. For the model calibration, the background roughness was set using a uniform value (Chézy u=80, v=60) on the whole mesh without differences between zones, since Zarzuelo et al. (2018) observed that including the spatial variability of this coefficient did not improve the goodness of the calibration. For turbulence closure, a K-epsilon model with constant values for horizontal and vertical viscosity was used. For the initial conditions, water at rest and null heat fluxes were used, employing a spin-up interval of one month to warm up the model.

The shortwave propagation module was used to assess the penetration of the waves from the continental shelf into the bay. This module is based on the SWAN model (Booij et al., 1999; Ris et al., 1999), a spectral wave model that solves the action balance equation considering wave-current interactions. It considers wave generation by wind and energy dissipation by whitecapping, wave breaking and bottom friction. For this module, spectral offshore boundary conditions were used with 3 h-interval data from Buoy 2342. Wind data from this buoy with the same interval were used as spatially uniform forcing to consider the energy exchange between wind and short waves.

The wave spectrum definition was limited to 24 frequencies between 0.05 and 1 Hz with 36 specified directions (15° steps). Physical processes such as whitecapping (Komen et al., 1984), depth-induced wave breaking (Battjes and Janssen, 1978), bottom friction (Hasselmann et al., 1973) and triads (Eldeberky and Battjes, 1996) were taken into account, but quadruplets were neglected. Both the wave and hydrodynamic modules were coupled and run simultaneously to consider the wave-current interactions: water levels and currents were included in the action balance equation of the wave module, whereas the wave-generated forces obtained by the wave module were included in the momentum balance of the hydrodynamic module.

https://doi.org/10.5194/essd-2022-467
Preprint. Discussion started: 11 January 2023

The model domain covers the Atlantic Ocean from Rota to Sancti-Petri, including the Bay of Cádiz, the two freshwater rivers (San Pedro and Guadalete) and the tidal creeks (Carracas and Sancti-Petri) (Fig.1). The grid defined for the hydrodynamic simulations has a spatial resolution ranging from 10 x 10 m in the area of the creeks to 5 x 5 m at the offshore boundary with a total of 90405 nodes. The vertical structure of the grid was implemented using a sigma-layer approach, for which the layer thickness is defined as a constant proportion of the total water depth. In this case, 10 layers with thicknesses of 2, 10, 10, 10, 10, 10, 10, 10, 10 and 2 % of the water depth were used. This number of layers was proven to be sufficient to capture vertical processes, as shown by Zarzuelo et al. (2018, 2021), since stratification is not important in bay dynamics. The grid for the wave module was based on the hydrodynamic grid, but with a lower resolution in creek areas where the role of waves is negligible (Zarzuelo et al., 2020), allowing a more efficient numerical scheme.

The offshore bathymetric data were provided by the Instituto Hidrográfico de la Marina (Spanish Ministry of Defense), while the detailed multibeam 2011 bathymetry of the bay was provided by the Bay of Cádiz Port Authority. The bathymetry of Sancti-Petri and Carracas Creeks was corrected with nautical charts. Finally, the topography was obtained from the 2010 digital terrain model of the Andalusian Regional Government with a resolution of 10×10 m^2, combined in the intertidal zones with 2015 LIDAR data with 2×2 m^2 resolution.

The results of the numerical model were extracted in a total of 553 observation nodes distributed along the bay (Fig.1b). To capture the variability, the results were obtained by working only with history files (nodes) but defining a large number of observation points and a high temporal resolution of the output data. The variables included water level, currents, density, significant wave height, peak period and wave direction.

3.2.2 Calibration and testing

The model calibration and testing were performed using the data from the mounted fields 2012 and 2013 surveys (Field2012 and Field2013, Table 1), respectively. Waves, currents (residual and instantaneous), water levels, temperature, and salinity were analyzed by means of correlation and skills coefficients. In the case of temperature, salinity and instantaneous currents, these variables were tested for both the 3D and depth averaged values. All measurements were checked visually and corrected for outliers and suspect data points whenever possible. The 9 locations where field and numerical data were compared are shown in Fig.2; full validation of the DELFT3D modeling approach is documented in Zarzuelo et al. (2015, 2020, 2021). Fig.2 depicts the correlation and skill coefficients for water levels, east and north velocities, residual currents projected on the axis of the channel, temperature, salinity and significant wave height.

Fig.3 shows the agreement of the temperature and salinity, the two variables with the lowest correlations, between the measured and modeled results. It can be observed that mean values are properly captured by the model, whereas the outliers reduce the agreements.

https://doi.org/10.5194/essd-2022-467
Preprint. Discussion started: 11 January 2023

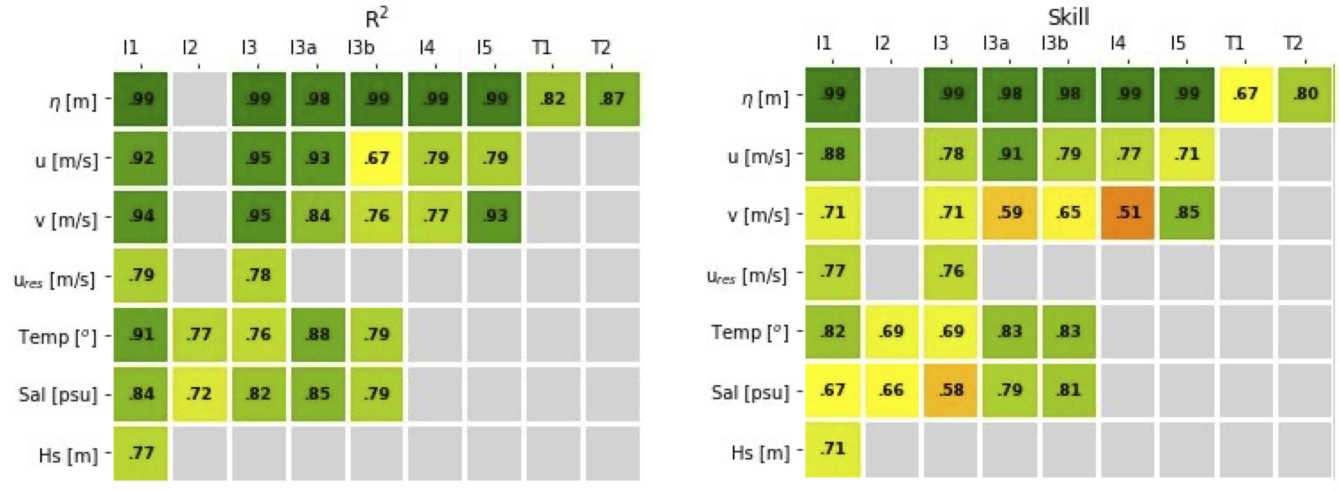

Figure 2. (a) Correlation coefficient (R^2) and (b) skill coefficient of the water level, east and north instantaneous velocity, residual velocity, temperature, salinity and wave height for each station. Color indicates the degree of acceptance (green excellent agreement, yellow–orange good agreement and red poor agreement).

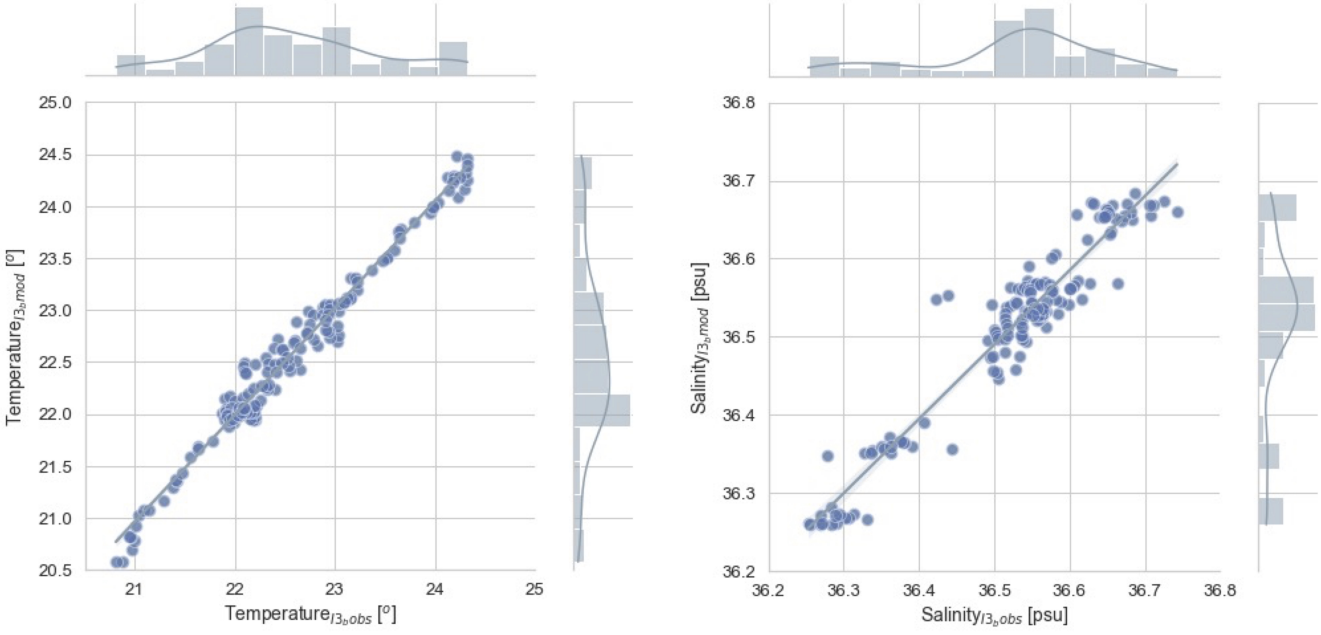

Figure 3. Test results of the temperature (a) and salinity (b) for location I3b.

https://doi.org/10.5194/essd-2022-467
Preprint. Discussion started: 11 January 2023

4 Data overview

The hybrid dataset obtained by applying the methodology described above has been used by the authors of this paper for different research applications, such as an analysis of the exchange flow between the main areas of the bay (Zarzuelo et al., 2022a), a characterization of seasonal dynamics and the influence of the sea-water heat exchange on bay dynamics (Zarzuelo et al., 2020), and an assessment of the impacts of recent human interventions on the estuarine dynamics (Zarzuelo et al., 2022a). In this section, an analysis of the spatial, fortnightly and seasonal variabilities is demonstrated as an example of the capabilities and potential of the hybrid dataset. In addition, storm surges recorded during the winter of 2013 (higher winds) were selected to analyze the relationship of wind intensity-direction with water density changes.

4.1 Data record

Representative stations where the numerical results were obtained with a high time resolution (10 min) were used to analyze the bay dynamics from intratidal to seasonal scales (Fig.1). The length of the records for the different stations, together with the variables measured, is shown in Fig.4. Some data gaps for the variables measured with the ADCPs (water levels, flow and wave data) occurred at the I1, I2 and I3 locations. During these gaps, only density measured with the CT instruments was recorded. The data gaps were caused by malfunctions or maintenance of the instruments.

4.2 Spatial variability

Fig.5 depicts the results from the analysis of the spatial variability of the main tidal and wave characteristics along the bay. The amplitude (Fig.2b) and phase (Fig.2c) of the main tidal constituent (M2) were calculated via a harmonic analysis of the depth-averaged flow velocities obtained at each station of the transect defined in Fig.2a using the numerical model for the 13-month simulation in 2012-2013 (Fig.4). Fig.2d shows the maximum significant wave height obtained with the same simulation at every station. Regarding the flow velocities, for the M2 amplitude, the highest values (1.5 m/s) are found where the Puntales channel connects with the inner basin, decreasing to almost zero (25-32 km) at the connection between the Carracas and Santi-Petri Creeks. In addition, an increase of 0.5 m/s is observed just at the entrance of the Puntales channel (10 km) and the tidal channels (21 km). These variations, related to the convergence and divergence processes of tidal wave propagation across the bay, are revealed by the spatial and temporal resolutions of the numerical model results.

The tidal phase of the M2 constituent is related to the celerity of the tidal wave and how it changes during its propagation through the bay. The period of constituent M2 (12.42 hours) is the time required for the phase to complete a 360° cycle. Thus, a phase of 200° corresponds to a wave tide propagation time of 6.9 hours. When the tidal wave enters the Puntales channel, the phase increases dramatically by 100° (3 hours). Then, the phase remains constant from the inner basin to the entrance of the creeks, from which it decreases almost linearly. It is also interesting to highlight the change that occurs around kilometer 30, since, as observed in previous studies (Zarzuelo et al., 2019), there is a point in the interior of the channels where the wave slows down. Finally, Fig.2d shows how wind waves dissipate when propagating from the two connections of the bay with the

https://doi.org/10.5194/essd-2022-467
Preprint. Discussion started: 11 January 2023

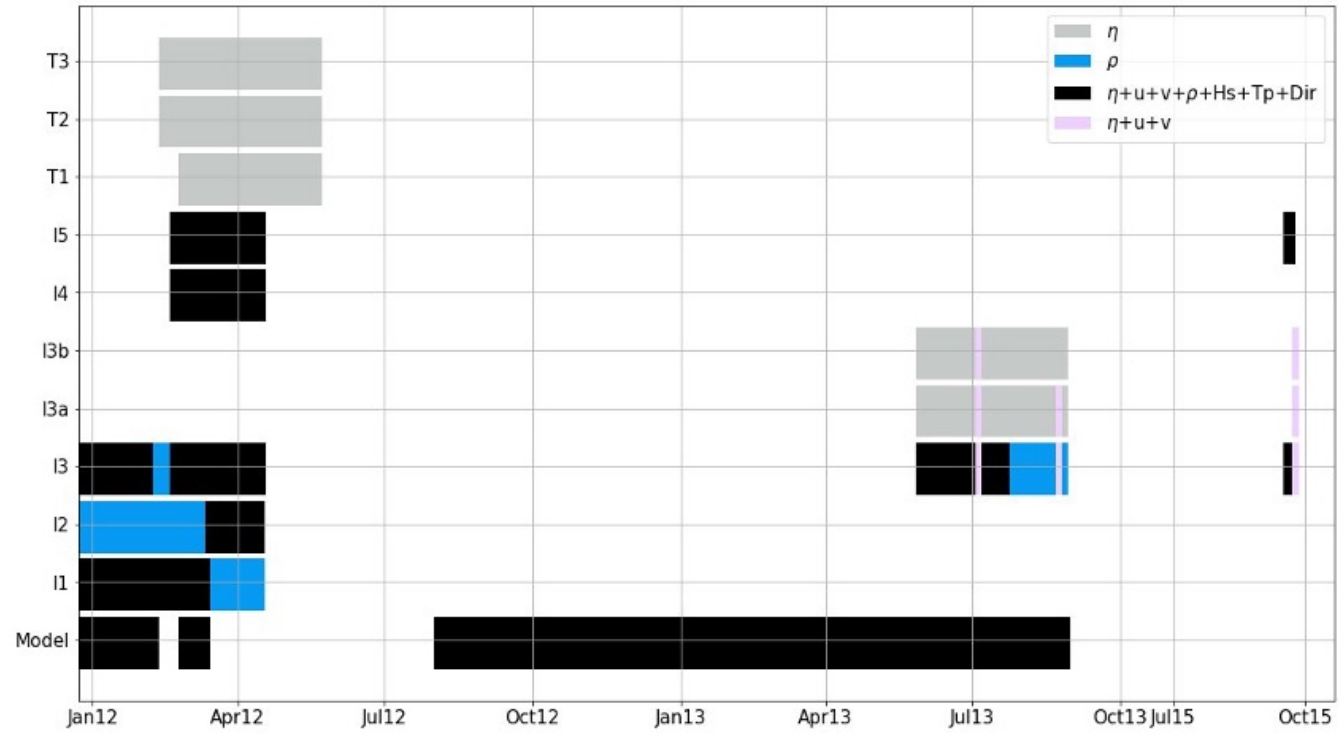

Figure 4. Extent of the valid data recorded by the monitoring station and the numerical model data during all field surveys. Vessel-towed observations are represented in purple. Bottom-mounted observations are represented in black (ADCP and CT), blue (CT) and gray (tidal gauge and velocity sensor failures).

285 open ocean to its interior, where their contribution is negligible in the Puntales channel, the inner basin and the Carracas and Sancti-Petri Creeks.

4.3 Fortnightly variability

The hybrid dataset also provides insights into the fortnightly variability of the semidiurnal species along cross-sections of the Puntales channel. This type of analysis is useful to assess the tidal prism or water exchange between the two basins connected
290 by this channel. Fig.6 depicts the amplitude of the semidiurnal species (D2) for the horizontal velocity of the flow obtained during the Neap2013 and Spring2013 surveys. The values are more than twice as high during spring tides, with maximum values in the deepest zones (0.15 and 0.4 m/s for neap and spring tides, respectively). If we analyze the density profiles measured during the same surveys, it is worth noting the decrease in density (0.4 kg/m^3) during the flood period, possibly coming from the seawater of the ocean (inverse estuary, as we can see in Fig.7b). This analysis is relevant to understanding the
295 change in density as the tide propagates and changes from flood to ebb and can even establish the location of the pycnocline, which could be done by obtaining numerical model data for more sections along the Puntales channel.

https://doi.org/10.5194/essd-2022-467
Preprint. Discussion started: 11 January 2023

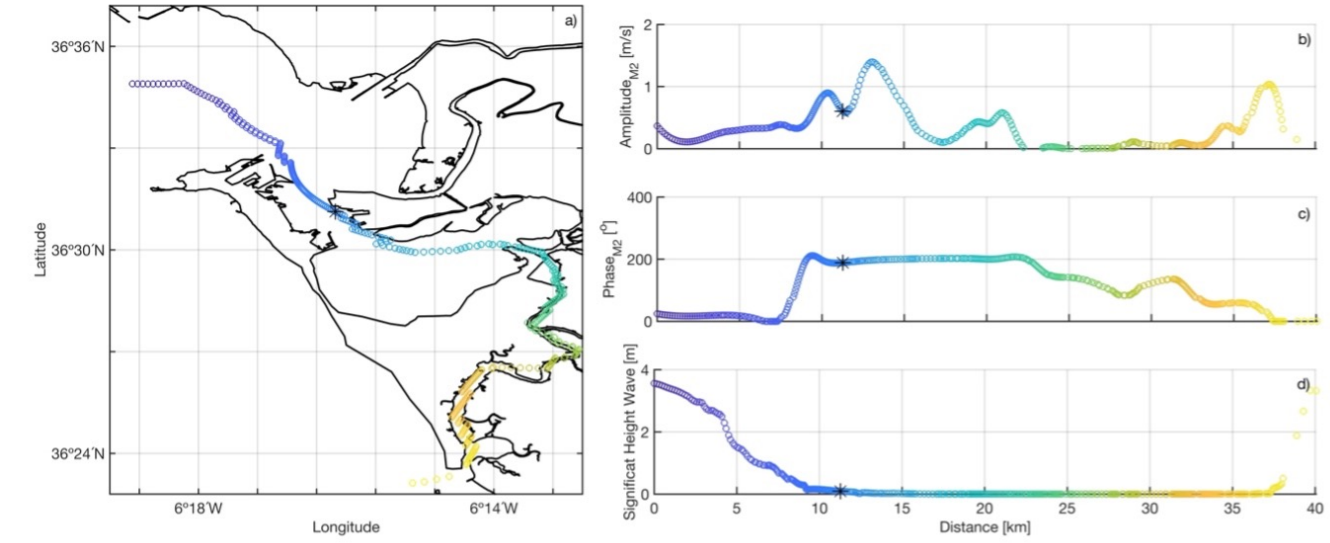

Figure 5. Panel a) represents the location of the points along the channel. The amplitude and phase of the tidal current constituents of the M2 along-channel are represented in Panels b) and c), respectively. Panel d) shows the variation in the significant height wave along the channel. The dot color indicates the distance. The asterisk corresponds to the location of the I3 instrument.

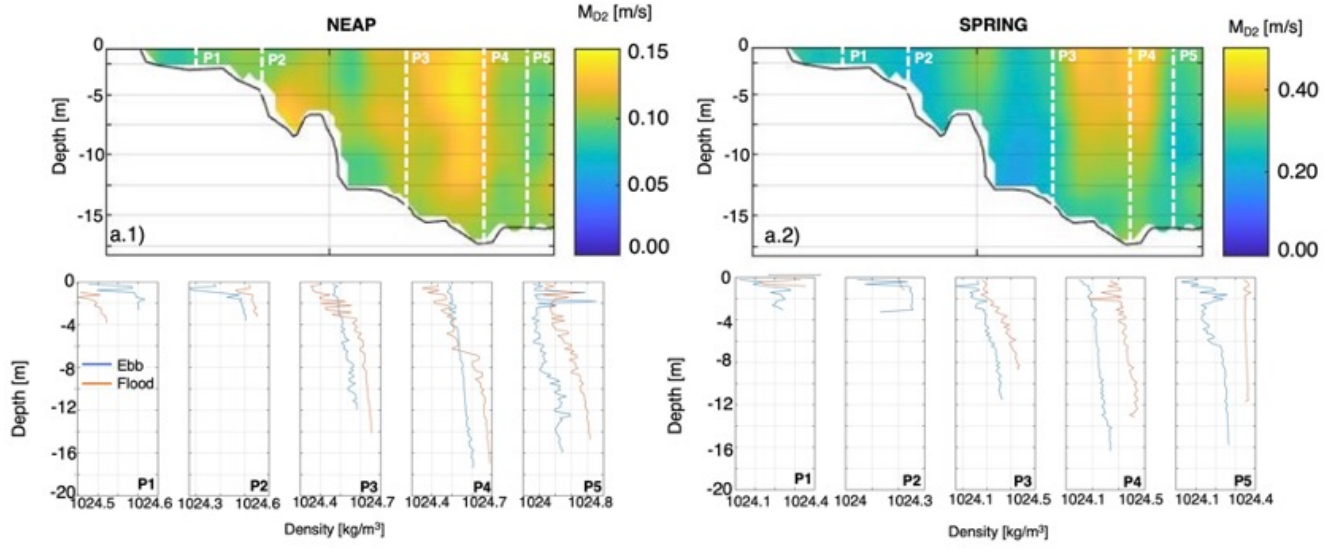

Figure 6. Amplitude of tidal species D2 of the current during Neap2013 (a.1) and Spring2013 (a.2). Second rows represent the density profile during Neap2013 and Spring2013 at maximum flood (orange line) and ebb (blue line).

https://doi.org/10.5194/essd-2022-467
Preprint. Discussion started: 11 January 2023

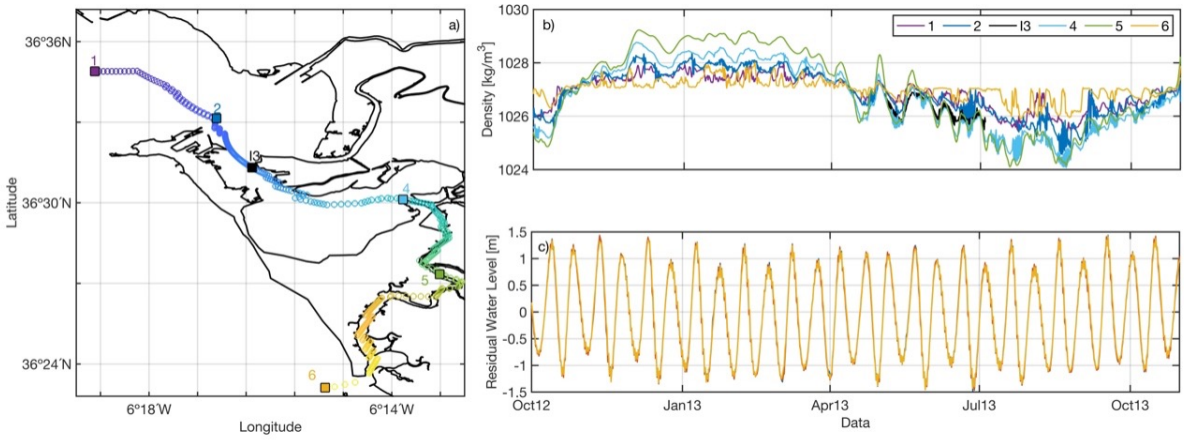

Figure 7. Panel a) represents the location of 5 points selected to show the seasonal variability of the density (b) and the residual water level (c). The data observed for I3 are plotted as a black line.

4.4 Seasonal variability

Of all the points obtained from the numerical model, 5 points were selected (Fig.7a) to facilitate representation. The density and residual water level time series data are displayed in Fig.7b and Fig.7c, respectively (October 2012– October 2013), together with observed records of the CT and ADCP located at I3. At this yearly scale, seasonal temperature variations are expected. Pronounced and rapid density variations in summer are induced by the alternation of warm westward countercurrents that characterize ocean circulation. In addition, it is important to note that in the winter months, the inner basin is denser than the outer basin (3 kg/m^3). This tendency changes in summer, when the inner basin becomes less dense (2 kg/m^3). Subtidal variability in the numerical data is well evidenced at a fortnightly time scale (Fig.7c). Larger density values are also clearly observed at spring tide for 1, 2, 3 and 4.

4.5 Extreme weather events

A wide range of weather conditions were captured during the measurements; in this section, we selected extreme wind events, as we observed in Zarzuelo et al. (2021) (winter period, Fig.8), to analyze how the density pattern changes according to the intensity and direction of the wind inside the bay. The same transect of Figs. 5 and 7 is selected for the first 20 kilometers that coincide with the entrance to the creeks. Two well-marked density patterns are identified during this winter period. The former can be observed when the density remains practically constant throughout the bay, coinciding with wind velocities below 5 m/s. However, the latter pattern corresponds to an increase in density of 2 kg/m^3 between the outer and inner basins (orange rectangle, Fig.8) that is observed when mean wind velocities are approximately 10 m/s, and the incoming directions are from the north (1,2,4) and west (3).

https://doi.org/10.5194/essd-2022-467
Preprint. Discussion started: 11 January 2023

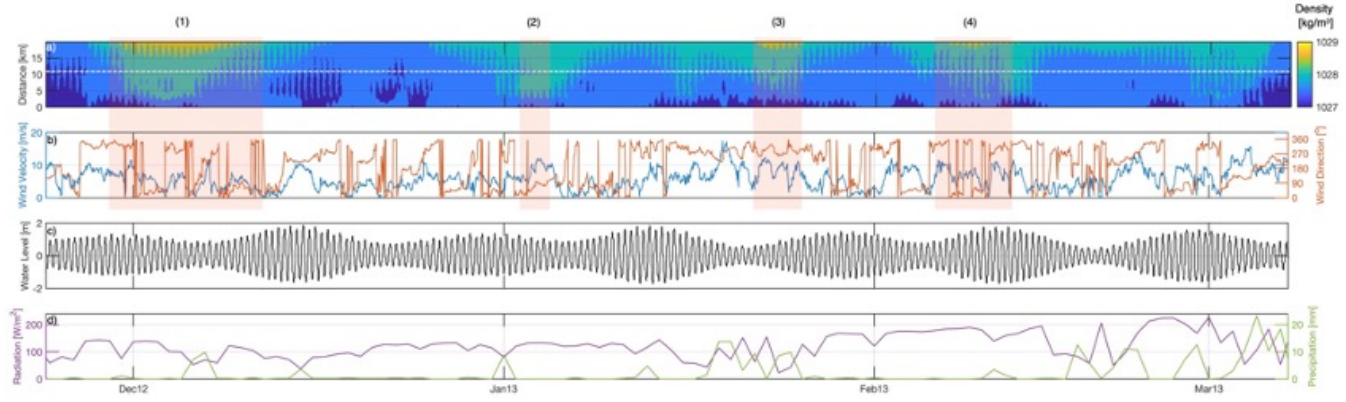

Figure 8. Panel (a) corresponds to the density variability along extreme wind events (winter period), and Panel (b) represents the wind velocity (blue line) and direction (orange line). The white dashed line corresponds to the location of instrument I3. The orange rectangle represents density changes throughout the bay. Panel (c) and Panel (d) represent the water level, and radiation (purple line) and precipitation (green line) recorded in the Bay of Cádiz, respectively.

As seen in Fig.7b, the estuary is an inverse one with denser seawater during winter; winds from the north and northwest introduce denser water into the inner basin. However, when there are no such winds, the bay is completely well mixed. In addition, changes in the density pattern may be related to other variables, such as water level (Fig.8c) or increased precipitation/radiation (Fig.8d).

5 Data availability

The data presented in this article are freely available at the ZENODO repository. See https://doi.org/10.5281/zenodo.7484187 (Zarzuelo et al., 2022b). The datasets are published in NetCDF format (.nc) with the observed and modeled results. The observed data files (water level, current, density and wave climate) are referred to with explicit file names and include extensive information (in header) about the site, instruments, setup and units.

The probe time series data are organized into five data files depending on the field survey:

- Mounted Field2012: 22 December 2011 to 20 April 2012
- Mounted Field2013: 15 May 2013 to 22 August 2013
- Mounted Field2015: 16 September 2015 to 22 September 2015
- Neap2013 and Spring2013: Neap tide 7 July 2013 and Spring tide 22 August 2013
- Neap2015: Neap tide 22 September 2015

https://doi.org/10.5194/essd-2022-467
Preprint. Discussion started: 11 January 2023

The numerical data files (water level, water current, wave climate and density) are organized into several data files from September 2012 to October 2013 to the points described in Fig.1.

6 Conclusions

A unique and comprehensive dataset is presented, containing bathymetric, water level, current, density and wave climate data from the Bay of Cádiz (southern Spain). The data have a high spatial and temporal resolution and capture a wide range of climate conditions in the bay, including storm events. The high-frequency data are suitable for testing intrawave-scale models, where the spatial coverage allows comparison with larger-scale wave-resolving models.

This high-resolution dataset allows the analysis of intrawave processes in this complex environment, including the influence of tidal currents on wave transformation (de Wit et al., 2019). Different applications can be extracted due to the measured and modeled variables. As seen in Section 4, application can provide the following: (1) an analysis of the spatial variability of the main tidal and wave characteristics along the bay, (2) the seasonal variability of the density and water level along the bay and throughout a whole year and (3) an analysis of how the density patterns vary according to wind events or according to the variability of the water level or other variables such as radiation or precipitation, among others.

The dataset can evaluate other variables or applications as a result of the obtained parameters. For example, these data provide the opportunity to analyze the influence of wind, waves and tidal flow on bed shear stresses, which are important for sediment transport. Moreover, the combination of ecological and physical data can be used to develop and verify (conceptual) models that describe interactions between biotic and abiotic processes. Ultimately, the dataset can be used to assess different scenarios such as future sea level rise and to support global warming mitigation and adaptation strategies.

Author contributions. CZ contributed to article compositions, article figures, article concept, maintain the station, analyse and organize the data sets, set up numerical modeling of DELFT3D and testing of DELFT3D. ALR contributed to set up numerical modeling of DELFT3D, model result processing and analysis, and lineage design. MB contributed to project initiation, article compositions, article figures, proof-reading and article figures and concept. MOS contributed to directed the monitoring activities project initiation, supervising, proofreading and the article concept.

Competing interests. The authors declare no competing interests.

Acknowledgements. This work has been supported by the Spanish Ministry of of Economy and Competitiveness, PID2021-125895OA-I00 (RESILIENCE), and by Department of Economy, Knowledge, Business and Universities of the Andalusian Regional Government (Project A-TEP-88-UGR20).

https://doi.org/10.5194/essd-2022-467
Preprint. Discussion started: 11 January 2023

M. Bermúdez gratefully acknowledges funding from FEDER/Junta de Andalucía-Consejería de Transformación Económica, Industria, Conocimiento y Universidades: Project B-TEP-110-UGR20 and from EU's Horizon 2020 Programme under Marie Skłodowska-Curie Grant Agreement 754446 and UGR Research and Knowledge Transfer Fund—Athenea3i.

https://doi.org/10.5194/essd-2022-467
Preprint. Discussion started: 11 January 2023

References

Alahmed, S., Ross, L., and Smith, S.: Coastal Hydrodynamics and Timescales in Meso-Macrotidal Estuaries in the Gulf of Maine: a Model Study, Estuaries and Coasts, pp. 1–21, 2022.

Allison, E. H., Kurien, J., and Ota, Y.: The human relationship with our ocean planet, 2020.

Asari, N., Suratman, M. N., Mohd Ayob, N. A., and Abdul Hamid, N. H.: Mangrove as a Natural Barrier to Environmental Risks and Coastal Protection, in: Mangroves: Ecology, Biodiversity and Management, pp. 305–322, Springer, 2021.

Baar, A., Boechat Albernaz, M., Van Dijk, W., and Kleinhans, M.: Critical dependence of morphodynamic models of fluvial and tidal systems on empirical downslope sediment transport, Nature communications, 10, 1–12, 2019.

Battjes, J. A. and Janssen, J.: Energy loss and set-up due to breaking of random waves, Coastal Engineering Proceedings, pp. 32–32, 1978.

Besada, V., Bellas, J., Sánchez-Marín, P., Bernárdez, P., and Schultze, F.: Metal and metalloid pollution in shelf sediments from the Gulf of Cádiz (Southwest Spain): Long-lasting effects of a historical mining area, Environmental Pollution, 295, 118 675, 2022.

Booij, N., Ris, R. C., and Holthuijsen, L. H.: A third-generation wave model for coastal regions: 1. Model description and validation, Journal of geophysical research: Oceans, 104, 7649–7666, 1999.

D'Alpaos, A.: The mutual influence of biotic and abiotic components on the long-term ecomorphodynamic evolution of salt-marsh ecosystems, Geomorphology, 126, 269–278, 2011.

de Wit, F., Tissier, M., and Reniers, A.: Characterizing wave shape evolution on an ebb-tidal shoal, Journal of Marine Science and Engineering, 7, 367, 2019.

Del-Rosal-Salido, J., Folgueras, P., Bermudez, M., Ortega-Sanchez, M., and Losada, M. A.: Flood management challenges in transitional environments: Assessing the effects of sea-level rise on compound flooding in the 21st century, Coastal Engineering, 167, 103 872, 2021.

Downing, J.: Twenty-five years with OBS sensors: The good, the bad, and the ugly, Continental Shelf Research, 26, 2299–2318, 2006.

Eldeberky, Y. and Battjes, J. A.: Spectral modeling of wave breaking: Application to Boussinesq equations, Journal of Geophysical Research: Oceans, 101, 1253–1264, 1996.

Eryani, I. and Nurhamidah, N.: Sedimentation management strategy in river estuary for control the water damage in downstream of Ayung River, International Journal on Advanced Science, Engineering and Information Technology, 10, 743–748, 2020.

Garel, E. and Ferreira, Ó.: Multi-year high-frequency physical and environmental observations at the Guadiana Estuary, Earth System Science Data, 7, 299–309, 2015.

Gartner, J. W. and Walters, R. A.: Tidal and residual currents in south San Francisco Bay, California: results of measurements, 1981-83, vol. 86, US Geological Survey, 1986.

Gill, A. and Adrian, E.: Atmosphere-ocean dynamics, Academic press, 30, 1982.

Gracia, F., Alonso, C., and Abarca, J.: Geomorphology and historical evolution of salt exploitations in salt marshes. Examples from the bay of Cadiz, CUATERNARIO Y GEOMORFOLOGIA, 31, 45–72, 2017.

Haasnoot, M., Brown, S., Scussolini, P., Jimenez, J. A., Vafeidis, A. T., and Nicholls, R. J.: Generic adaptation pathways for coastal archetypes under uncertain sea-level rise, Environmental Research Communications, 1, 071 006, 2019.

Haro, S., Jesus, B., Oiry, S., Papaspyrou, S., Lara, M., González, C., and Corzo, A.: Microphytobenthos spatio-temporal dynamics across an intertidal gradient using Random Forest classification and Sentinel-2 imagery, Science of The Total Environment, 804, 149 983, 2022.

https://doi.org/10.5194/essd-2022-467
Preprint. Discussion started: 11 January 2023

Hasselmann, K., Barnett, T. P., Bouws, E., Carlson, H., Cartwright, D. E., Enke, K., Ewing, J., Gienapp, A., Hasselmann, D., Kruseman, P., et al.: Measurements of wind-wave growth and swell decay during the Joint North Sea Wave Project (JONSWAP)., Ergaenzungsheft zur Deutschen Hydrographischen Zeitschrift, Reihe A, 1973.

Hobohm, C., Schaminée, J., and van Rooijen, N.: Coastal habitats, shallow seas and inland saline steppes: ecology, distribution, threats and challenges, in: Perspectives for Biodiversity and Ecosystems, pp. 279–310, Springer, 2021.

Hopkinson, C. S., Wolanski, E., Cahoon, D. R., Perillo, G. M., and Brinson, M. M.: Coastal wetlands: A synthesis, in: Coastal Wetlands, pp. 1–75, Elsevier, 2019.

Jiménez-Arias, J. L., Morris, E., Rubio-de Inglés, M. J., Peralta, G., García-Robledo, E., Corzo, A., and Papaspyrou, S.: Tidal elevation is the key factor modulating burial rates and composition of organic matter in a coastal wetland with multiple habitats, Science of The Total Environment, 724, 138 205, 2020.

Kitheka, J. U.: Coastal tidally-driven circulation and the role of water exchange in the linkage between tropical coastal ecosystems, Estuarine, Coastal and Shelf Science, 45, 177–187, 1997.

Komen, G., Hasselmann, S., and Hasselmann, K.: On the existence of a fully developed wind-sea spectrum, Journal of physical oceanography, 14, 1271–1285, 1984.

Lane, A.: The heat balance of the North Sea, Proudman Oceanographic Laboratory, 8 (46), 1989.

LEE, H.-J., CHAO, S.-Y., FAN, K.-L., WANG, Y.-H., and LIANG, N.-K.: Tidally induced upwelling in a semi-enclosed basin: Nan Wan Bay, Journal of Oceanography 53:, pp. 467–480, 1997.

Legaz, M., de León, S. P., and Soares, C. G.: Validation of a spectral wave model for wave energy assessments in the bay of Cádiz, in: Developments in Renewable Energies Offshore, pp. 38–44, CRC Press, 2020.

Lesser, G. R., Roelvink, J. v., van Kester, J. T. M., and Stelling, G.: Development and validation of a three-dimensional morphological model, Coastal engineering, 51, 883–915, 2004.

Li, P., Li, G., Qiao, L., Chen, X., Shi, J., Gao, F., Wang, N., and Yue, S.: Modeling the tidal dynamic changes induced by the bridge in Jiaozhou Bay, Qingdao, China, Continental Shelf Research, 84, 43–53, 2014.

Lobo, F., Plaza, F., González, R., Dias, J., Kapsimalis, V., Mendes, I., and Río, V. D. d.: Estimations of bedload sediment transport in the Guadiana Estuary (SW Iberian Peninsula) during low river discharge periods, Journal of Coastal Research, pp. 12–26, 2004.

Meyer-Peter, E. and Müller, R.: Formulas for bed-load transport, in: IAHSR 2nd meeting, Stockholm, appendix 2, IAHR, 1948.

Miró, J., Megina, C., Donázar-Aramendía, I., Reyes-Martínez, M., Sánchez-Moyano, J., and García-Gómez, J.: Environmental factors affecting the nursery function for fish in the main estuaries of the Gulf of Cadiz (south-west Iberian Peninsula), Science of The Total Environment, 737, 139 614, 2020.

Morales, J., Delgado, I., and Gutierrez-Mas, J.: Sedimentary characterization of bed types along the Guadiana estuary (SW Europe) before the construction of the Alqueva dam, Estuarine, Coastal and Shelf Science, 70, 117–131, 2006.

Newton, A., Icely, J., Cristina, S., Brito, A., Cardoso, A. C., Colijn, F., Dalla Riva, S., Gertz, F., Hansen, J. W., Holmer, M., et al.: An overview of ecological status, vulnerability and future perspectives of European large shallow, semi-enclosed coastal systems, lagoons and transitional waters, Estuarine, Coastal and Shelf Science, 140, 95–122, 2014.

Nielsen, P.: Analysis of natural waves by local approximations, Journal of Waterway, Port, Coastal, and Ocean Engineering, 115, 384–396, 1989.

O'brien, S.: On Marangoni drying: nonlinear kinematic waves in a thin film, Journal of Fluid Mechanics, 254, 649–670, 1993.

https://doi.org/10.5194/essd-2022-467
Preprint. Discussion started: 11 January 2023

Purkiani, K., Becherer, J., Klingbeil, K., and Burchard, H.: Wind-induced variability of estuarine circulation in a tidally energetic inlet with curvature, Journal of Geophysical Research: Oceans, 121, 3261–3277, 2016.

Reeve, D., Chadwick, A., and Fleming, C.: Coastal engineering: processes, theory and design practice, CRC Press, 2018.

Ris, R., Holthuijsen, L., and Booij, N.: A third-generation wave model for coastal regions: 2. Verification, Journal of Geophysical Research: Oceans, 104, 7667–7681, 1999.

Schoen, J. H., Stretch, D. D., and Tirok, K.: Wind-driven circulation patterns in a shallow estuarine lake: St Lucia, South Africa, Estuarine, Coastal and Shelf Science, 146, 49–59, 2014.

Shang, J., Sun, J., Tao, L., Li, Y., Nie, Z., Liu, H., Chen, R., and Yuan, D.: Combined effect of tides and wind on water exchange in a semi-enclosed shallow sea, Water, 11, 1762, 2019.

van Maren, D. S. and Cronin, K.: Uncertainty in complex three-dimensional sediment transport models: equifinality in a model application of the Ems Estuary, the Netherlands, Ocean Dynamics, 66, 1665–1679, 2016.

Van Rijn, L. C.: Unified view of sediment transport by currents and waves. I: Initiation of motion, bed roughness, and bed-load transport, Journal of Hydraulic engineering, 133, 649–667, 2007.

Weisscher, S. A., Boechat-Albernaz, M., Leuven, J. R., Van Dijk, W. M., Shimizu, Y., and Kleinhans, M. G.: Complementing scale experiments of rivers and estuaries with numerically modelled hydrodynamics, Earth Surface Dynamics, 8, 955–972, 2020.

Yang, Z., Wang, T., Voisin, N., and Copping, A.: Estuarine response to river flow and sea-level rise under future climate change and human development, Estuarine, Coastal and Shelf Science, 156, 19–30, 2015.

Zarzuelo, C., Díez-Minguito, M., Ortega-Sánchez, M., López-Ruiz, A., and Losada, M. Á.: Hydrodynamics response to planned human interventions in a highly altered embayment: The example of the Bay of Cádiz (Spain), Estuarine, Coastal and Shelf Science, 167, 75–85, 2015.

Zarzuelo, C., López-Ruiz, A., Díez-Minguito, M., and Ortega-Sánchez, M.: Tidal and subtidal hydrodynamics and energetics in a constricted estuary, Estuarine, Coastal and Shelf Science, 185, 55–68, 2017.

Zarzuelo, C., López-Ruiz, A., and Ortega-Sánchez, M.: Impact of human interventions on tidal stream power: The case of Cádiz Bay, Energy, 145, 88–104, 2018.

Zarzuelo, C., D'Alpaos, A., Carniello, L., López-Ruiz, A., Díez-Minguito, M., and Ortega-Sánchez, M.: Natural and human-induced flow and sediment transport within tidal creek networks influenced by ocean-bay tides, Water, 11, 1493, 2019.

Zarzuelo, C., López-Ruiz, A., and Ortega-Sánchez, M.: Beyond human interventions on complex bays: Effects on water and wave dynamics (study case Cádiz Bay, Spain), Water, 12, 1907, 2020.

Zarzuelo, C., López-Ruiz, A., and Ortega-Sánchez, M.: The Role of Waves and Heat Exchange in the Hydrodynamics of Multi-Basin Bays: The Example of Cádiz Bay (Southern Spain), Journal of Geophysical Research: Oceans, 126, e2020JC016 346, 2021.

Zarzuelo, C., López-Ruiz, A., Valle-Levinson, A., Díez-Minguito, M., and Ortega-Sánchez, M.: Bridge-piling modifications on tidal flows in an estuary, Coastal Engineering, 173, 104093, 2022a.

Zarzuelo, C., López-Ruiz, A., Bermúdez, M., and Ortega-Sánchez, M.: Hydrodynamic data for the Bay of Cádiz (southern Spain), https://doi.org/10.5281/zenodo.7484187, 2022b.

https://doi.org/10.5194/essd-2022-467
Preprint. Discussion started: 11 January 2023

Open Access Earth System Science Data Discussions

Instrument	Location	Field Survey	Height above bed	Settings	Wave measurements
ADCP (2MHz) +OBS	I1	Field2012	0.5 m	2 min bursts every 15 min, bin size 0.5 m	17 min bursts every 120 min, bin size 1 m, 1 Hz
CT	I1	Field2012	0.3 m	15 min	
ADCP (1MHz)	I2	Field2012	0.7 m	2 min bursts every 15 min, bin size 0.5 m	17 min bursts every 60 min, bin size 1 m, 1 Hz
CT	I2	Field2012	0.3 m	1 sample every 15 min	
ADCP (1MHz)	I3	Field2012	0.7 m	2 min bursts every 15 min, bin size 0.75 m	17 min bursts every 60 min, bin size 2 m, 1 Hz
CT	I3	Field2012	0.3 m	1 sample every 15 min	
ADCP (0.6MHz)	I3	Field2013	1.3 m	1 min bursts every 30 min, bin size 1 m	17 min bursts every 240 min, bin size 4 m, 1 Hz
CT	I3	Field2013	0.6 m	1 sample every 15 min	
ADCP (0.6MHz)	I3	Field2015	1.3 m	0.5 min bursts every 5 min, bin size 1 m	17 min bursts every 60 min, bin size 4 m, 1 Hz
CT	I3	Field2015	0.6 m	1 sample every 5 min	
ADCP (2MHz)	I3a	Field2013	1.0 m	1 min bursts every 15 min, bin size 1 m	17 min bursts every 120 min, bin size 1 m, 1 Hz
CT	I3a	Field2013	0.6 m	1 sample every 15 min	
ADCP (2MHz)	I3b	Field2013	1.0 m	1 min bursts every 15 min, bin size 1 m	17 min bursts every 120 min, bin size 1 m, 1 Hz
CT	I3b	Field2013	0.6 m	1 sample every 15 min	
ADCP (2MHz)	I4	Field2012	0.5 m	2 min bursts every 15 min, bin size 0.5 m	17 min bursts every 60 min, bin size 1 m, 1 Hz
ADCP (2MHz)	I5	Field2012	0.5 m	2 min bursts every 15 min, bin size 0.5 m	17 min bursts every 60 min, bin size 1 m, 1 Hz
ADCP (1MHz)	I5	Field2015	1.2 m	0.5 min bursts every 5 min, bin size 1 m	17 min bursts every 60 min, bin size 2 m, 1 Hz
CT	I5	Field2015	0.6 m	1 sample every 5 min	
Tidal Gauge	T1	Field2012	0.1 m	10 sec bursts every 15 min, 1 Hz	
Tidal Gauge	T2	Field2012	0.1 m	10 sec bursts every 15 min, 1 Hz	
Tidal Gauge	T3	Field2012	0.1 m	10 sec bursts every 15 min, 1 Hz	

Table 1. The mooring deployments for bottom-mounted surveys.